Electron acceleration by an Alfvénic pulse propagating in an auroral plasma cavity

F. Mottez, Vincent Génot

Electron acceleration by an Alfvénic pulse propagating in an auroral plasma cavity

F. Mottez[1] and V. Génot[2]

Laboratoire Univers et Théories (LUTH), Observatoire de Paris, CNRS, Université Paris Diderot, 5 place Jules Janssen, 92190 Meudon, France. (fabrice.mottez@obspm.fr)

IRAP, Université de Toulouse (UPS) & CNRS (UMR5277), Toulouse, France. (vincent.genot@cesr.fr)

[1]Laboratoire Univers et Théories
(LUTH), Observatoire de Paris, CNRS,
Université Paris Diderot, 5 place Jules
Janssen, 92190 Meudon, France.

[2]IRAP, Université de Toulouse (UPS) &
CNRS (UMR5277), Toulouse, France.

Abstract. With the help of a 2.5D Particle In Cell (PIC) simulation code, we investigate the physics of the acceleration of auroral electrons, through the interaction of an isolated Alfvén wave packet with a plasma density cavity. The cavity is edged by density gradients perpendicular to the magnetic field. We show that a single passing of an isolated wave packet over a (infinite) cavity creates an electron beam. It triggers local current and beam-plasma instabilities, and small scale coherent electric structures. The energy flux of downgoing electrons is significantly increased, whereas upgoing electrons are also accelerated, even if no beam is formed. Accelerated electrons remain after the passage of the Alfvénic pulse, allowing the observation of energetic particles without any significant electromagnetic perturbation. The dependence of this process on the electron to ion mass ratio is consistent with its control by inertial effects.

1. Introduction

Early models of auroral particle acceleration were based on quasi-static parallel electric fields, accelerating electrons and ions in opposite directions, with roughly the same narrow distribution in energy [*Block and Falthammar*, 1990]. Other evidences of accelerated electrons, with broader distributions in energy and direction, have shown the importance of time-varying electric fields [*Hultqvist et al.*, 1988], possibly carried by Alfvén waves [*Kletzing et al.*, 1994]. Deep plasma cavities above the Earth auroral zone are a privileged place for electron acceleration [*Hilgers et al.*, 1992] and the subsequent turbulence, characterized by electrostatic coherent structures such as double layers and solitary waves [*Bostrom et al.*, 1988; *Eriksson et al.*, 1997]. With the Freja spacecraft, is was shown that these regions are pervaded by Alfvén wave packets (termed as Solitary Kinetic Alfvén Waves, SKAW). Measurements have shown that these waves carry a Poynting flux large enough to accelerate electrons at auroral energies if this flux is to be efficiently dissipated through a relevant mechanism [*Louarn et al.*, 1994; *Volwerk et al.*, 1996]. Coincident satellite measurements of fields and particles demonstrate that, as functions of increasing auroral activity, 25-39% of the total electron energy deposited in the ionosphere may be attributed to the action of Alfvén waves [*Chaston et al.*, 2007]. *Hull et al.* [2010] performed a case study of the development of an acceleration region based on multi-point Cluster observations in the high altitude auroral zone, across the plasma sheet and into the polar cap. They first identify an Alfvén wave dominated system, with its typical broad spectrum of accelerated particles, in the vicinity of a plasma cavity. After Alfvénic acceleration the signature (the so-called inverted V) of particles accelerated by a quasi-static structure, such as a

strong double layer is observed. This suggest that the Alfvénic acceleration process could act as a precursor to the quasi-static process. These phenomenons were associated to a poleward boundary intensification of the auroral arcs seen by an ultraviolet camera. *Hull et al.* [2010] performed an analysis of the small-scale Alfvénic currents and noticed that, in the inertial dispersive range, they are damped. In their conclusion, the authors suggest that this might be due to Landau damping, near and above the high altitude acceleration region. In the present paper we propose a different interpretation: the current attenuation would be the result of a transfer of energy from the wave to the electrons, with the local heating of electrons, and formation of accelerated electron beams, associated to the generation of a parallel (to the ambient magnetic field) electric field.

There is a precise reason why this Alfvénic current dissipation through electron acceleration would occur at the inertial scale. According to the MHD theory, an Alfvén wave could not accelerate particles along the ambient magnetic field $\vec{B}_0$ because the parallel electric field ($E_\parallel$) is null. Within the MHD framework, wavelengths are long compared to the inertial length c/ω_{pe} and to the ion Larmor radius ρ_i, i.e. $k_\perp c/\omega_{pe} << 1$ or $k_\perp \rho_i << 1$, where $k_\perp$ is the perpendicular (to $\vec{B}$) wave vector, ω_{pe} is the electron plasma frequency, c is the speed of light, and ρ_i is the ion Larmor radius ($\rho_i = m_i v_{ti}/eB$, m_i is the ion mass). Beyond the MHD approximation, there exists two regimes of parameters where Alfvén waves can carry a parallel electric field. This is when $k_\perp c/\omega_{pe} \sim 1$ or $k_\perp \rho_i \sim 1$ [*Goertz*, 1984]. In the Earth auroral zone, the plasma beta $\beta = 2\mu_0 p/B_0^2 \ll m_e/m_i$, and one deduces that $\rho_i \omega_{pe}/c = (\beta m_i/m_e)^{1/2} < 1$; the condition $k_\perp c/\omega_{pe} \sim 1$ is then reached before $k_\perp \rho_i \sim 1$. At such scales, an Alfvén wave carries a parallel electric field, given for a plane wave by the relation:

$$\frac{E_\parallel}{E_\perp} \sim \frac{k_\parallel}{k_\perp} \frac{\left(\frac{c}{\omega_{pe}} k_\perp\right)^2}{1 + \left(\frac{c}{\omega_{pe}} k_\perp\right)^2} \tag{1}$$

This parallel electric field has a functional form similar to those of the other fields, i.e. sinusoidal, with the same wavelength.

Therefore, most of the theories of auroral acceleration by waves are based on inertial Alfvén waves (see for instance *Kletzing et al.* [1994]; *Lysak et al.* [1996]; *Watt et al.* [2008]). Bridging with the early models cited at the beginning of the introduction, we can see now that the time varying electric fields associated to the non stationary acceleration structures [*Hultqvist et al.*, 1988] are, in many cases, identified as inertial Alfvén wave electric fields.

Before concluding that such waves can accelerate electrons, one must question the origin of the oblique component $k_\perp$ of the wave vector. An explanation based on the properties of plasma cavities has been proposed [*Génot et al.*, 1999]. When an Alfvén wave, initially in pure parallel propagation ($k_\perp = 0$), propagates upon a perpendicular density gradient, the wave front is bent (phase mixing) as propagation is faster in the low density region than the denser one. In that case, there is a parallel electric field quite similar to the one of an inertial Alfvén wave: in the above formula, $k_\perp$ may be replaced by $\partial_x \ln n$ (n is the plasma density, and ∂_x is a spatial derivative perpendicularly to the magnetic field). The role of density cavities on the formation of narrow-scale Alfvén waves has been confirmed recently with a three dimensional linear model of the auroral flux tube [*Lysak et al.*, 2008].

Therefore the parallel electric field could be partly explained by a propagation effect of Alfvén waves on the borders of the plasma cavities, where the perpendicular density gradients are large.

A set of numerical simulations showed that parallel electric fields first develop on the (rather long) Alfvén wavelength and accelerates strongly a minority of electrons [*Génot et al.*, 2000]. Then an unstable electron beam is formed which triggers current and beam instabilities. The non-linear evolution shows the formation of electron holes structures and associated coherent (small scale) electrostatic structures observed in auroral cavities by many spacecraft [*Génot et al.*, 2001, 2004]. More recently a comparative study conducted with FAST data [*Chaston et al.*, 2006] revealed that predictions of the present model were actually observed (electron acceleration on the density gradients, wave focusing in the cavity, ...). On the simulation side, analog results were found independently by *Tsiklauri et al.* [2005]. However these simulations were initialized with a sinusoidal AW (one wavelength covering the parallel length of the simulation domain), whereas observed SKAW propagate as isolated wave packets (see for instance observations by the Freja spacecraft in *Louarn et al.* [1994]; *Volwerk et al.* [1996]). To obtain a quantification of the acceleration process according to the previous scenario for more realistic conditions, it is therefore crucial to wonder whether a localized input (the Alfvén pulse) may still trigger sufficient acceleration to power the aurora, i.e. whether energy transfer from the wave to the electrons may still take place over a reduced distance along field lines. The present paper is addressing this broad question by analysing the propagation of Alfvén wave packets upon a density gradient. Investigating the process at work in such a configuration with the help of a kinetic code which retains non-linearities (for a description of the PIC code see *Mottez et al.* [1998]), we shall set a bridge between the work of *Génot et al.* [1999] which included a localized Alfvénic pulse, but considered only the bi-fluid

approach (via linearized equations), and the self-consistent work of *Génot et al.* [2004] where Alfvén waves were purely sinusoidal.

The numerical method and the sets of simulation parameters are given in Section 2 whereas the pulse propagation is tested in Section 3. Electron and ion acceleration are evidenced in Section 4.1, followed in Section 4.2 by an analysis of the plasma turbulence generated by accelerated electrons. In Section 4.3, we determine which part of the wave spectrum contributes most efficiently to the acceleration. Section 5 is devoted to the discussion of our results compared to other similar, but contradicting, simulations [*Tsiklauri*, 2007], and we conclude in Section 6.

2. Numerical method and parameters

Following *Génot et al.* [2000, 2001, 2004] the numerical simulations make use of an electromagnetic PIC code that takes into account the motion of the electron guiding center and the full ion motion [*Mottez et al.*, 1998].

The 2D simulation domain is defined by the rectangular coordinate system (x, y). The direction x is the direction of the ambient magnetic field B_0 and corresponds to the longest side of the simulation domain. The vectors are tri-dimensional, with a component z perpendicular to the simulation box.

The physical variables are reduced to dimensionless variables. Time (the inverse of) and frequencies are normalized by the electron plasma frequency ω_{p0} which corresponds to a reference background electron density n_0. Velocities are normalized to the speed of light c, and the magnetic field is given in terms of the dimensionless electron gyrofrequency ω_{ce}/ω_{p0}. The mass unit is the electron mass m_e. Therefore, the units are c/ω_{p0} for distances, ω_{p0}/c for wave vectors, e for charges, en_0 for the charge density, $c\omega_{ce}/\omega_{p0}$

for the electric field, and ce/ω_{p0} for the magnetic moment μ of the electrons. In the following parts of the paper, all equations, numerical values and figures are expressed in this system of units. Let us note that the reference density n_0 (or plasma frequency ω_{p0}) is a free parameter and may therefore be fixed arbitrarily; other plasma parameters are consequently deduced from this choice. For instance, setting $n_0 = 10$ cm^{-3} leads to $B_0 = 4\mu$T for a magnetization given by $\omega_{ce}/\omega_{p0} = 4$ typical of the auroral region.

We present results from six simulations : run A to run F. Run A is set initially with an Alfvén wave packet which propagates upon an homogeneous plasma. The other simulations are set with Alfvén waves (a wave packet or a sinusoidal wave) which propagate in an infinite plasma cavity extended along the magnetic field direction, and delimited by two strong density gradients perpendicular to the magnetic field.

The simulations are initialized with the sum of 8 (or 1) sinusoidal waves with a maximum at $x = 0$. The waves have a right-hand circular polarization. In run A and run B, $\delta B_y(x)$ at t=0 is a sum of eight sinus of equal amplitude and $\delta B_z(x)$ the sum of eight cosines of the same amplitude, given by the wave magnetic field $\delta B = 0.032 \times B_0$ where $B_0 = 4.0$ is the background magnetic field amplitude (or $\omega_{ce}/\omega_{p0} = 4$). In run D and run E a single sinusoidal wave is initially set with an amplitude $\delta B = 0.0904 \times B_0$, such that the runs A, B, D, E have the same initial magnetic energy. (The sum $\Sigma_i \delta B_i^2$ has the same value in the four simulations, where i is the index of the monochromatic waves that contribute to the wave packet.) Setting the same magnetic energy in these simulations allows for a better comparison of the energy transfer from the waves to the particles, because, at least in the MHD approximation, the wave Poynting flux of AW, $S = S_{\parallel} = \delta B^2 V_A/\mu_0$, is proportional to the magnetic energy density δB^2.

In run A and run B, wavelengths are $\lambda = \lambda_0/m$ where $\lambda_0 = 409.6$ and m varies from 1 to 8. Only the larger wavelength of run B is kept in run D, while the smallest is kept in run E. The phase velocities vary from 0.4529 for the shortest wave to 0.2257 for the longest, i.e. the dispersion is non-negligible. **The ideal MHD Alfvén velocity is $V_A = B/\sqrt{\mu_0\rho} = 0.2$ is smaller; it does not represent accurately the propagation of these waves for which inertial effects are effective.** The polarization of the 8 sinusoidal waves is described in details in the appendix of [*Mottez*, 2008].

The size of the whole simulation domain is $4096\Delta x \times 128\Delta y$, where $\Delta x = \Delta y = 0.1$ is the size of the grid cells.

Mottez [2003] have shown, in the context of Vlasov-Maxwell formalism, that the gradients of the auroral plasma cavity can be modelized as tangential discontinuities, in spite of a non-scalar pressure tensor that cannot be characterized through the MHD theory [*Mottez*, 2004]. Run B contains a plasma cavity whose area of largest depth, $n_{min}/n_{max} = 0.2$ is a channel of infinite length, and $12\Delta y$ broad. The edges of the cavity are smoothed with a gaussian profile. The electron thermal velocity (in and outside the cavity) is $v_{te} = 0.1$ (ion and electron temperatures are equal). The ion to electron mass ratio is varied from $m_i/m_e = 100$ (run C) to $m_i/m_e = 400$ (in runs A, B, D, E). There are $\sim 26 \times 10^6$ particles of each species corresponding to an average of 50 particles per cell. There are 2048 time steps in the simulation, defined by $\Delta t = 0.2$, corresponding to a time lapse $t_{max} = 409.6$.

3. Test bench for the pulse propagation

The pulse propagation in a uniform plasma has been tested with the simulation run A. Figure 1 shows the $E_y(x, y(x,t), t)$ transverse component of the electric field along the direction x, as a function of time for this simulation. Initially, the line defined by

$y(x,0) = 5$ is in the middle of the density gradient. Displacing it with the same velocity as the plasma allows to keep it inside the region of transverse density gradient. Therefore, considering the MHD approximation, we move this line with the velocity $\vec{v} = \vec{E} \times \vec{B}/B^2$. Practically, $y(x,t)$ is the solution of $d_t y(x,t) = E_z(x,y,t)/B_x(x,y,t)$.

We can see that the superposition of the 8 waves is like a single Alfvénic pulse (and a residual short wavelength sinusoidal wave). It propagates with dispersion, but on the timescale of the simulation, we can still clearly identify a wave packet. (A longer simulation box and more computing time would allow for longer wavelengths, and a less dispersive Alfvén wave packet, as in MHD.) Initializing the wave packet with a sum of 8 waves with an amplitude distribution fitting a Gaussian shape, instead of a sum of 8 waves of equal amplitudes, would make a smoother and better localized wave packet. Nevertheless, wave packets observed on-board satellites, such as in [*Louarn et al.*, 1994], do not specifically exhibit a Gaussian shape.

In run A, the initial density is uniform. It is not the case for other simulations. The electron density in run B is shown on the Fig. 2, for three different times t_i corresponding to the beginning, (approximately) the middle and the end of the simulation. To help the reader to understand the Fig. 3, we have drawn the line $y(x,t_i)$ on Fig. 2. Figure 2 shows that the perpendicular displacement of the cavity maximizes where the wave packet amplitude also maximizes. This motion is magnified by the aspect ratio of the figure (corresponding to dimensions 409.6×12.8), it is actually less important than it looks on the figure. We can see on Fig. 2 that to a good approximation, the iso-density areas follow the two $y(x,t)$ lines superimposed to the gradient. This proves that the motion of the cavity is mainly controlled by the $\vec{E} \times \vec{B}/B^2$ drift of the plasma induced by the (Alfvénic

pulse) electromagnetic field as expected. Is the cavity depth and profile modified by the Alfvénic pulse ? On Fig. 2, we can compare, for instance the cavity at time $t = 0$ (for any value of x since it is initially uniform in that direction), and at time $t = 409.6$. At this late time, the Alfvénic pulse is in the middle of the simulation box (around $x = 200$), and we can see that for $x < 200$, where the pulse has already passed, the cavity has the same depth and the same transverse shape (i.e. along the y axis) as at $t = 0$. In other words, the passage of the wave packet does not destroy the plasma cavity. This confirms the results shown in previous works, conducted with only one sinusoidal wave [*Génot et al.*, 2001, 2004]. It is at odds with *Sydorenko et al.* [2008] in which numerical simulations of an Alfvén wave packet of high amplitude propagating in the ionospheric Alfvén resonator are conducted. Contrary to the present work, they initialized a wave with a transverse wave vector. The particle motion is computed under more restrictive simplifications as in our code, but, reciprocally, their simulations include a real mass ratio and longitudinal density gradients, where our simulations are initially homogeneous along the ambient magnetic field direction. As expected in the inertial Alfvén wave regime, acceleration occurs. This acceleration is accompanied, for small enough wavelength (its does not work with the fundamental mode), by the creation of a density depletion in a small area at low altitude, where the accelerating parallel electric field reaches its highest amplitude. The density depletion is caused here by the accelerated plasma being expelled from the acceleration region (a depression of about 50% may be formed). In our simulation, the acceleration process does not destroy the cavity, but it does not dig it either. This may be a consequence of the homogeneity of the plasma in the longitudinal direction, that is also the direction of plasma acceleration.

Figure 3 shows $E_y(x, y(x,t), t)$ for run B. The waves are the same as in run A, but they are set upon the density channel. The situation becomes more complex, because their polarization is those of Alfvén waves uniquely for the density outside the cavity. Inside the cavity, other wave modes can be triggered. We can see that some waves are emitted backward, especially for short wavelengths. Nevertheless, the figure is still dominated by the Alfvén wave packet that propagates from left to right. As we can see, there is more dispersion than in run A. In the end of run B, the wave packet is still recognizable, but is severely affected. **We can see on that figure that the pulse has traveled across a distance of 200, over a duration of 409. The corresponding velocity is $v_P \sim 0.5$. This is the value that we adopt in the following parts of the present paper, when we need to characterize the pulse propagation velocity.**

4. Quantification of the acceleration

4.1. Particle energy flux

The significant difference between run A and run B concerns the parallel electric field. In run A (not shown) it is absent. In run B, no parallel electric field is set initially, but it develops naturally, as a consequence of the phase mixing on the density gradients. A map of the parallel electric field $E_x(x, y)$ is shown on Fig. 5 for three different times. From an initial vanishing value, a localized structure develops as the Alfvénic pulse propagates. The E_x electric field is mainly localized in and around the density depletion, and its structure is time dependent. This evolution may also be traced on Fig. 6 that displays $E_x(x, y(x,t), t)$. At time zero, it is null everywhere, but a bipolar structure soon emerges with the characteristic size of the wave packet. In the linear regime, the scale of the parallel electric field is given by the characteristic scale of the incoming field, E_y, as it can

be seen on Fig. 3. After time $t = 200$, small scale structures appear. This is a signature of a non-linear evolution of the system. We can notice first a peak of parallel electric field, that propagate at the same speed as the wave packet, soon followed by a bunch of less intense structures that propagate slightly slower, and preceded by small amplitude fast structures. All these structures emerge from the wave packet. The parallel electric field is able to accelerate electrons along the ambient magnetic field (x direction), as can be seen on Fig. 7. This figure shows the electron distribution function $f_e(x, v_x)$ integrated over y. The figure is in log-scale, it provides a good way to show the creation of a minority of fast electrons, with velocities v_x up to $8v_{te}$.

According to *Semeter et al.* [2001], the intensity of an auroral arc is quasi-proportional to the flux of electron kinetic energy across a surface, defined as an integral over the velocity space

$$F(x) = \int v'^2 v'_x f(\vec{v}', x, y') d^3\vec{v}' dy'. \tag{2}$$

To evaluate the efficiency of the acceleration process seen in the simulations, we have evaluated this flux. Practically, we compute a sum over the macro-particles,

$$F(x) = \Sigma_S v^2 v_x \tag{3}$$

where S is a subset of particles. Let x', y' be their coordinates, S is restricted to the particles such as $x_{min} < x' < x_{max}$. In order to have sufficient statistics, but a reasonable spatial resolution, we have chosen $x_{min} = x - 10\Delta x$ and $x_{max} = x + 10\Delta x$. In order to focus on the acceleration process, that happens essentially in and around the density depletion,

we have also computed fluxes for particles with y' in the middle half of the simulation box, (between $0.25L_y$ and $0.75L_y$). There is no selection of the particles based on their velocities. All the particles (thermal and suprathermal) are included in the computation of the flux.

We have computed four distinct components of the electron kinetic energy flux. They are F_{eu}, computed with the upgoing particles only, F_{ed} with downgoing particles only, F_{ecu} with the upgoing particles only with y' in the middle half of the simulation box (in and around the density channel), and F_{ecd} with downgoing particles only in the middle half of the box.

Figure 8 is a plot of the time evolution of these four components, for $x = 102.4$, in the simulation run B. Of course, as the centered fluxes F_{ecd} and F_{ecu} are computed with a smaller number of particles, their amplitude is smaller too (proportional to the ratio of the number of particles in the two areas; the two sets of particles have the same initial velocity distributions). We can see that at time 100, the wave packet approaches the surface $x = 102.4$, and a faint fluctuation of the fluxes appears. At time 200, the bulk of the Alfvénic pulse crosses the surface of interest, and this corresponds to the maximum of the flux intensification. Then, the fluxes decrease. When the pulse has left the surface of interest, the fluxes are higher than in the initial conditions, showing that the effect of the acceleration can be felt even after the pulse crossing. Comparing the centered fluxes F_{ecd}, F_{ecu} and the total fluxes F_{ed}, F_{eu}, we can see that the relative increase of flux is more pronounced in the middle of the box, on the density gradients, than just close to it. The flux F_{ecd} is increased by a factor 4.3, while F_{ed} is amplified by a 2.25 only. As there are less particles in the middle than on the sides of the cavity we conclude that the acceleration

occurs in the center of the box, the plasma cavity region. This confirms the role of the plasma cavity in the acceleration process.

The comparison of the upward and of the downward fluxes shows that the acceleration occurs in the two directions, but mainly in the direction of propagation of the Alfvénic pulse, i.e. downward. If this was a resonant process of acceleration, we would have only acceleration for particles with a velocity close to the Alfvénic pulse velocity (i.e. downward). The observation of an upward flux shows that the process involved here is not purely resonant. Nevertheless, the fact that downward acceleration is more efficient is somehow resonant, as it is due to the fact that the particles with an initially downward velocity see the accelerating electric field carried by the wave during a longer time than the upgoing particles.

Figure 9 is a similar plot for the proton energy fluxes. We can see that the ions are accelerated. The flux of the downward protons increases by a factor 1.6. It is 2.7 times less than for the electrons. Proton distribution functions (not shown) do not exhibit any ion beam; this is consistent with a weaker acceleration efficiency for the protons. On Fig. 9, we can also notice that the difference between upward and downward energy fluxes is smaller than for the electrons. This is due to the fact that the difference of upward and downward ion velocities is smaller than for the electrons. When it is compared to the Alfvén wave packet velocity, we have $2v_{te}/v_P \sim 0.36$ for the electrons, and $2v_{ti}/v_P \sim 0.018$ for the ions, where we have taken $v_P = 0.5$ for the wave packet. Therefore, the difference of time spent by the upgoing and the downgoing ions in the acceleration region (that moves with the waves) is weak compared to the case of the electrons, and the upgoing and the downgoing ion accelerations have approximately the same efficiency. *Tsiklauri et al.* [2005] made a

series of simulations, in the context of Solar physics, that presents similarities with the simulations presented here and in previous papers (see [*Mottez et al.*, 2006] for a detailed comparison). In [*Tsiklauri et al.*, 2005], plots of the ion distribution functions show a broadening that is not seen in our simulations. In Run A for instance, we can see only an increase by 5% of the ion perpendicular thermal speed. Actually, when *Tsiklauri et al.* [2005] analyzed the contribution of this broadening to the energy budget, they found no contribution, because the kinetic energies in the directions y and z oscillate in anti-phase. Therefore, they conclude that there is no ion acceleration in their simulations and that the ion distribution broadening is due to the usual velocity perturbations associated to the AW. Why is there a distribution broadening in their simulations, and not in ours ? In [*Mottez*, 2008], the perturbation of the velocity fields associated to the AW is given, in the frame of the cold bi-fluid plasma theory. This is the perturbation used for the initial conditions of the simulations of the present study. The ion velocity perturbations (given in code units) are

$$V_{py}(x) \; = \; Sc_{p1}B_y(x) \text{ and } V_{pz}(x) = c_{p1}B_z(x) \tag{4}$$

where $c_{p1} = -Sm_e/(\omega + S\omega_{ci})k\omega m_p$ where $S = \pm 1$ depends on the polarization (right or left-handed). We can see that for a weak ion to electron mass ratio (16 in [*Tsiklauri et al.*, 2005]) this perturbation is strong, while for a larger mass ratio (400 in the present study), the ion velocity perturbation is lower. Therefore, we can conclude that there is no significant ion acceleration in the present simulations, and this result agrees with the analysis conducted by other authors.

Where are the accelerated electrons ? On Fig. 7 there is a peak of high energy electron density at the same (moving) location as the wave packet. **In order to localize the**

positions of the accelerated electrons within the wave packet, we invite the reader to compare Fig. 7 with Figures 4 and 5 that display the perpendicular ($E_y(x,y)$) and parallel ($E_x(x,y)$) electric fields at the same times. The electrons can reach a velocity $0.8 = 8v_{te}$, and the wave packet velocity is $v_P \sim 0.5$, therefore many of the accelerated electrons propagate, at least temporarily, in front of the wave packet. Actually, a comparison with Fig. 4 shows that the wave packet, as seen with E_y is very extended. On the contrary, the parallel electric field E_x, seen on Fig. 5, has a very localized structure with peaks of high amplitude spread over a distance ~ 50 only (the smaller peaks of parallel electric field are discussed in section 4.2). At time 409, they are localized around $x = 200$, and this is precisely where we can see, on Fig. 7, the largest number of accelerated particles. The population of accelerated particles extends on the two sides of this area, with the most energetic particles ahead of it. In that situation, a space probe passing below an acceleration region would measure the energetic downgoing electrons slightly before the parallel electric field of the Alfvén wave at the origin of their acceleration. This is possible only if the Alfvén wave velocity is comparable to the electron velocity (here $v_A \sim 3v_{te}$). This does not happen in the high altitude auroral zone (10 000 km) as seen for instance from the Viking, Cluster or Polar spacecrafts, where v_A is of the order of c, but it is possible at lowest altitudes (1000 km) in the regions that have been explored by Freja, for instance.

4.2. Coherent structures

We have seen on Fig. 6 that after time 200, the cascade from large scale to small scale parallel electric field structures becomes visible. This effect was already seen in previous

studies, with a sinusoidal Alfvén wave [*Génot et al.*, 2001, b]. When looking at Fig. 7, we can see that the small scale electric field structures are associated to vortices in the phase space. These vortices have a suprathermal velocity comparable to the wave packet velocity. Similarly to the analysis developed in *Génot et al.* [2004], we infer that they are a consequence of the nonlinear evolution of an electron beam plasma instability. The beam is formed by the fastest electrons which quit the acceleration region (the packet) ahead of it. To assess the triggering of this instability we use the criterion derived by *Gary* [1985]:

$$\frac{v_{the-beam}}{v_{drift-beam}} \ll \left(\frac{n_{e-beam}}{n_e}\right)^{1/3} \tag{5}$$

where $v_{the-beam}$ is the beam thermal velocity, $v_{drift-beam}$ is the beam drift velocity, n_{e-beam} is the beam density and n_e is the core density. Using the electron distribution function at time 179.2 and x =102.4 (see the second panel of Figure 7), for which small scale structures are already present, we deduce the following parameters: $v_{the-beam} = 0.04$, $v_{drift-beam} = 0.69$, $n_{e-beam} = 0.026$, and $n_e = 1.21$, which readily satisfy the above criterion.

Similarly to the small amplitude case studied in *Génot et al.* [2004] we do not observe signatures of a Buneman instability. This instability is a consequence of a large velocity drift of the electron distribution with respect to the ion one and is triggered in the presence of a parallel electric field of sufficiently large amplitude and installed on long spatial scale. This does not happen with a localized pulse of reasonable amplitude.

4.3. Efficiency

The wave packet is built initially as a sum of sinusoidal waves of various wavelengths with the same amplitude. This choice is arbitrary but facilitates the study of each wave mode efficiency in the acceleration process.

Run D was initialized with a single sinusoidal wave with the largest wavelength. Its amplitude was chosen in order to have the same initial wave energy as in runs A and B. No electron acceleration is observed in run D. On the contrary run E was initialized with a single sinusoidal wave, with the smallest wavelength. Fig 10 shows that it is an efficient electron accelerator. These two simulations indicate that the short Alfvén wavelengths contribute more efficiently to the electron acceleration. The issue is that the Alfvén wave with short wavelengths is more dispersive (the non dispersive waves correspond to the case of the long MHD wavelengths), and do not favour the coherence of the Alfvén wave packet over long distances. Therefore, for efficient acceleration by Alfvén wave packets, there is a balance to find, in terms of the size of the packets, between the dispersive effects, and the efficiency of the electron acceleration.

5. Influence of the ion to electron mass ratio

Within the MHD framework ($\omega \ll \omega_{ci}$) Alfvén waves constitute a single mode. It is actually the degeneration of two different modes, with right-hand and left-hand circular polarizations, whose dispersion relations become quite distinct at high frequencies. *Tsiklauri* [2007] performed simulations of acceleration by ion cyclotron waves, in the continuation of the left-hand polarized Alfvén wave branch. Our simulations are based on the propagation of right-hand polarized Alfvén waves, in the low frequency part of the whistler branch. We made this choice because the right-hand polarized waves are less dispersive, more like the MHD waves usually involved in the literature. In particular with

the right-hand polarized mode, nothing special happens at frequencies close to the ion cyclotron frequency. The observations of Solitary Kinetic Alfén Waves encourage us to think that, in the auroral zone, Alfvén wave packets are only weakly dispersive. For left-hand polarized waves with a small wavelength -i.e. ion cyclotron waves- the case is different. The dispersive **nature** of the propagation constitutes an important aspect of the problem, because the ion cyclotron frequency corresponds to a resonance. ***Tsiklauri*** **[2007] has shown a coupling between the parallel electric field and the perpendicular electric field driven by the Alfvén wave, that, for the left-hand polarized mode is strongly influenced by ion gyrofrequency effects**, with important consequences on the acceleration process. This is what he observed in his simulation, based on left-hand polarized waves. As the ion cyclotron frequency is inversely proportional to the ion to electron mass ratio, in order to characterize this resonnant effect, *Tsiklauri* [2007] performed several simulations in which the ion to electron mass ratio was varied. A result was that the acceleration process is less efficient with a higher ion to electron mass ratio, and they concluded that the acceleration is not controlled by the ion polarization drift amplitude (as with inertial Alfvén waves) but by the ion cyclotron frequency. This is contrary to the interpretation developed in the present paper, and we explore below this contradiction.

The inertial effect is caused by the ion polarization drift, that is proportional to the ion mass m_i, and by the electron inertia, that is proportional to the inverse of the electron mass m_e^{-1}. Therefore, the inertial effects are a growing function of the ion to electron mass ratio. Therefore, a test on the dependency of the acceleration on the mass ratio helps to discriminate the control by the gyrofrequency (growing with m_e/m_i) from the

control by inertial effects (growing with m_i/m_e). Following *Tsiklauri* [2007], we have conducted a series of numerical simulations with the same parameters as in run B, except for the mass ratio. Fig 11 shows the time evolution of the maximum value of the parallel electric field E_x, for simulations run B ($m_i/m_e = 400$), run F ($m_i/m_e = 200$), run C ($m_i/m_e = 100$). In our simulations with right-hand polarized waves, it appears that when we increase the mass ratio, the growth of the parallel electric field is more significant. This property is compatible with the predominance of the inertial effect on the Alfvén wave propagation. Figure 12 shows the energy flux of the downward electrons. Here again, we observe a larger electron acceleration for the largest mass ratio (400). The comparison of the acceleration for mass ratios of 100 and 200 is not so simple. Anyway, we do not observe that the acceleration is more efficient with a decreasing mass ratio. Our results are therefore different from those of *Tsiklauri* [2007]. Nevertheless, there is no contradiction in the physics, since we do not explore the same branch of wave propagation. Let us note that both our work and those by *Tsiklauri* [2007] were conducted with reduced ion to electron mass ratio. We can expect that for the real mass ratio, the efficiency of the acceleration by right-hand polarized waves would be better than in run B. On the contrary, the acceleration provided through a cyclotron wave would be weaker, loosing importance among the auroral acceleration processes. Of course, modifying the mass ratio also changes the ion cyclotron period, as well as the Alfvén velocity to electron thermal velocity ratio, that are important in both kinds of acceleration processes. Therefore, this simple test alone does not assess whether the process underlying acceleration in the simulations of the present paper is indeed caused by inertial effect. It simply gives a clue,

in response to *Tsiklauri* [2007]'s numerical experiments. A more thorough study of the influence of the mass ratio will be proposed in a forthcoming study.

6. Discussion and conclusion

In this paper, we have confirmed that an Alfvénic pulse propagating downward along a plasma cavity is able to generate transverse small scales, and thanks to inertial effect, a parallel electric field. This parallel electric field causes a broad spectrum of accelerated electrons, mainly in the downward direction. The electrons are accelerated within the wave packet, but they can propagate faster, and be present at lower altitudes. The acceleration process increases the downward flux of kinetic energy of the electrons, and this should favour the triggering of optical auroras in the ionosphere. Short Alfvénic pulses (small wavelengths) accelerate the electrons more efficiently than long ones. A short study of the efficiency of the acceleration process as a function of the ion to electron mass confirms that the accelerating parallel electric field is compatible with inertial effects (inertial Alfvén wave triggered acceleration).

Watt et al. [2010] performed a series of numerical simulations to evaluate the efficiency of the shear Alfvén waves in providing the electron energy flux that powers the aurora. They used a self consistent drift-kinetic code which allows to simulate a significant portion of an auroral magnetic field line, taking into account the variations of the magnetic field strength and plasma density with altitude. By comparison, our simulation box is much smaller than that, and we do not take into account the convergence of the lines of force.

Watt et al. [2010] took into account the ion polarization drift which induces the Alfvén wave inertial effects, and produces, in their formulation, a scalar electric potential drop. Electrons are accelerated by a parallel electric force injected at the top of the simulation

box, which corresponds to those of an inertial Alfvén wave packet. Further effects depend on the propagation of this wave packet along the converging magnetic field lines, and the dynamics of the electrons. The authors have computed the electron energy flux, and they conclude that the input of energy given by the wave may be sufficient to excite detectable auroras (in three cases, over the four studied), for a detection threshold set at 1 $\mathrm{mW.m^{-2}}$. The amplitude of the wave packet injected at the upper boundary is quite strong, with an associated parallel electric potential drop of several hundreds of Volts. However their Figure 7 shows that about 80% of the Poynting flux associated with the wave disappear in the very first cells of their simulation box. The initialization procedure may be in cause: it seems that the the Alfvén wave electromagnetic field is included in the initial conditions, but not the associated perturbations of the electron and ion velocities. Therefore, we can expect that with a more consistent initialization of the Alfvén wave packet, the efficiency of the electron acceleration would be even better than claimed by the authors. The correct Alfvén polarization is established quickly, but at the expense of the initial amplitude of the wave electromagnetic field. Therefore, the true amplitude of the Alfvén wave in their simulation does not corresponds to the one set at time 0, and used as a reference.

Let us notice that the initial electron distribution in their simulations already contains an energetic tail, as it is modeled with a kappa distribution function. With the consideration of the plasma cavity interaction with the wave, the high energy tail of the electron distribution appears self-consistently.

Comparing the work of *Watt et al.* [2010] and ours it appears that our simulations offer an insight into the origin of the parallel electric field and the microscopic aspects of the

Alfvénic acceleration that cause auroras, while *Watt et al.* [2010] focus mainly on their macroscopic effects.

In both studies it is shown that an Alfvén wave packet can provide a significant increase of the electron energy flux, favoring the excitation of observable polar auroras.

The acceleration of electrons through the interaction of Alfvén waves and plasma cavities is not bound to happen only in the Earth auroral zone although the Earth environment is the only region where, up to now, Alfvénic processes have been observed in situ. Indeed, since the pioneering work of *Heyvaerts and Priest* [1983], many theoretical works have been devoted to Alfvénic acceleration on transverse density gradients in the Sun corona. Recent works have been specifically devoted to non-MHD effets [*Tsiklauri et al.*, 2005; *McClements and Fletcher*, 2009; *Bian and Kontar*, 2011]. There are also observational evidences that Alfvén waves can accelerate electrons in the vicinity of Io and Jupiter [*Hess et al.*, 2007] sometimes combined with other acceleration structures [*Hess et al.*, 2009]. However in the Jovian case, it is not obvious that the plasma cavities are the sources of the inertial effects [*Mottez et al.*, 2010] and it is possible that they result from wave filamentation at the border of the Io plasma torus [*Hess et al.*, 2010].

Up to now, we are not aware of any measurement of the length scale of the auroral cavities along the magnetic field. In our simulations, it has been considered as infinite. We plan to simulate the effect of Alfvénic pulses propagating over finite size auroral cavities, and evaluate the efficiency of the acceleration mechanism according to the ratio between the characteristic length scales of the cavity and of the Alfvénic pulse. We are also interested to see if waves of stronger amplitude can contribute to regenerate or to

destroy the plasma cavities. These topics are currently under study and will be presented in a forthcoming paper.

Acknowledgments. The authors acknowledge support from the Institut National des Sciences de l'Univers (INSU/CNRS) of France under the program PNST. The numerical simulations were performed at the computing center (DIO) of the Paris-Meudon observatory.

References

Bian, N. H. and Kontar, E. P., Mar, 2011, Parallel electric field amplification by phase mixing of Alfven waves. Astronomy & Astrophysics, 527, A130+, 10.1051/0004-6361/201015385.

Block, L. P., and Falthammar, C.-G. (1990), The role of magnetic-field-aligned electric fields in auroral acceleration, *J. Geophys. Res. 95* (14), 5877-5888.

Bostrom, R., Gustafsson, G., Holback, B., Holmgren, G., Koskinen, H., Jul. 1988. Characteristics of solitary waves and weak double layers in the magnetospheric plasma. Physical Review Letters 61, 82-85.

Chaston, C. C., Génot, V., Bonnell, J. W., Carlson, C. W., McFadden, J. P., Ergun, R. E., Strangeway, R. J., Lund, E. J., and Hwang, K. J. (2006), Ionospheric erosion by Alfvén waves, *J. Geophys. Res. 111*, Issue A3, CiteID A03206.

Chaston, C. C., Carlson, C. W., McFadden, J. P., Ergun, R. E., Strangeway, R. J. (2007), How important are dispersive Alfven waves for auroral particle acceleration?, *Geophys. Res. Lett. 34*, 7101-+.

Eriksson, A. I., Malkki, A., Dovner, P. O., Bostrom, R., Holmgren, G., Holback, B., (1997), A statistical survey of auroral solitary waves and weak double layers 2. Measurement accuracy and ambient plasma density, *Journal of Geophysical Research, 102*

(11), 11385-11398.

Gary, S. P. (1985), Electrostatic instabilities in plasmas with two electron components, J. Geophys. Res. 90, 8213-8221.

Génot, V., Louarn, P., Mottez, F., (2000), Electron acceleration by Alfven waves in density cavities. Journal of Geophysical Research (Space Physics) 105, 27611-27620.

Génot, V., Louarn, P., Mottez, F., (2001), Fast evolving spatial structure of auroral parallel electric fields. J. Geophys. Res. 106, 29633-29644.

Génot, V., Louarn, P., Mottez, F., (2004), Alfvén wave interaction with inhomogeneous plasmas: acceleration and energy cascade towards smallscales. Annales Geophysicae 6, 2081-2096.

Génot, V., Louarn, P., Le Quéau, D., Oct. 1999. A study of the propagation of Alfven waves in the auroral density cavities. Journal of Geophysical Research (Space Physics) 104 (13), 22649-22656.

Génot, V., Mottez, F., Louarn, P., Jan. 2001. Particle Acceleration Linked to Alfven Wave Propagation on Small Scale Density Gradients. Physics and Chemistry of the Earth C 26, 219-222.

Goertz, C. K., Nov. 1984. Kinetic Alfvén waves on auroral field lines. Planetary and Space Science, 32 1387-1392.

Hess, S., Mottez, F., Zarka, P., Nov. 2007. Jovian S burst generation by Alfven waves. Journal of Geophysical Research (Space Physics) 112 (11), 11212-+.

Hess, S., Mottez, F., Zarka, P., Jul. 2009. Effect of electric potential structures on Jovian S-burst morphology. Geophysical Research Letters 36, 14101-+.

Hess, S. L. G., Delamere, P., Dols, V., Bonfond, B., Swift, D., Jun. 2010. Power transmission and particle acceleration along the Io flux tube. Journal of Geophysical Research (Space Physics) 115 (14), 6205-+.

Heyvaerts, J. and Priest, E. R., Jan. 1983. Coronal heating by phase-mixed shear Alfven waves. Astronomy and Astrophysics 117, 220-234.

Hilgers, A., Holback, B., Holmgren, G., Bostrom, R., Jun. 1992. Probe measurements of low plasma densities with applications to the auroral acceleration region and auroral kilometric radiation sources. Journal of Geophysical Research (Space Physics) 97 (16), 8631-8641.

Hull, A. J., Wilber, M., Chaston, C. C., Bonnell, J. W., McFadden, J. P., Mozer, F. S., Fillingim, M., Goldstein, M. L., Jun. 2010. Time development of field-aligned currents, potential drops, and plasma associated with an auroral poleward boundary intensification. Journal of Geophysical Research (Space Physics) 115 (14), 6211-+.

Hultqvist, B., Lundin, R., Stasiewicz, K., Block, L., Lindqvist, P., Sep. 1988. Simultaneous observation of upward moving field-aligned energetic electrons and ions on auroral zone field lines. Journal of Geophysical Research (Space Physics) 93, 9765-9776.

Kletzing, C. A., Jun. 1994. Electron acceleration by kinetic Alfven waves. Journal of Geophysical Research (Space Physics) 99, 11095-11104.

Louarn, P.,Wahlund, J. E., Chust, T., de Feraudy, H., Roux, A., Holback, B., Dovner, P. O., Eriksson, A. I., Holmgren, G., 1994. Observation of kinetic Alfven waves by the Freja spacecraft. Geophys. Res. Lett. 21, 1847-+.

Lysak, R. L., Lotko, W., Mar. 1996. On the kinetic dispersion relation for shear Alfven waves. Journal of Geophysical Research (Space Physics) 101, 5085-5094.

563 Lysak, R. L., Song, Y., Oct. 2008. Propagation of kinetic Alfven waves in the ionospheric
564 Alfven resonator in the presence of density cavities. Geophys. Res. Lett. 35, 20101-+.
565 McClements, K. G. and Fletcher, L., Mar. 2009. Inertial Alfvén Wave Acceleration
566 of Solar Flare Electrons. The Astrophysical Journal 693, 1494-1499, 10.1088/0004-
567 637X/693/2/1494.
568 Mottez, F., Jun. 2003. Exact nonlinear analytic Vlasov-Maxwell tangential equilibria with
569 arbitrary density and temperature profiles. Physics of Plasmas 10, 2501-+.
570 Mottez, F., Sep. 2004. The pressure tensor in tangential equilibria. Annales Geophysicae
571 22 (9), 3033-3037.
572 Mottez, F. and Génot, V. and Louarn, P., Apr. 2006. Comment on "PIC simulations of
573 circularly polarised Alfvén wave phase mixing: a new mechanism for electron accel-
574 eration in collisionless plasmas" by Tsiklauri et al. Astronomy and Astrophysics 449,
575 449-450, 10.1051/0004-6361:20054229.
576 Mottez, F., Mar. 2008. A guiding centre direct implicit scheme for magnetized plasma
577 simulations. Journal of Computational Physics 227, 3260-3281.
578 Mottez, F., Adam, J. C., Heron, A., Oct. 1998. A new guiding centre PIC scheme for elec-
579 tromagnetic highly magnetized plasma simulation. Computer Physics Communications
580 113, 109-130.
581 Mottez, F., Hess, S., Zarka, P., Aug. 2010. Explanation of dominant oblique radio emission
582 at Jupiter and comparison to the terrestrial case. Planetary and Space Science 58, 1414-
583 1422.
584 Semeter, J., Vogt, J., Haerendel, G., Lynch, K., Arnoldy, R., Jul. 2001. Persistent
585 quasiperiodic precipitation of suprathermal ambient electrons in decaying auroral arcs.

586 Journal of Geophysical Research (Space Physics) 106, 12863-12874.

587 Sydorenko, D. and Rankin, R. and Kabin, K., Oct. 2008. Nonlinear effects in the iono-
588 spheric Alfvén resonator. Journal of Geophysical Research (Space Physics) 113, A12,
589 10206-+, 10.1029/2008JA013579.

590 Tsiklauri, D. and Haruki, T., Aug. 2008. Physics of collisionless phase mixing. Physics of
591 Plasmas 15, 112902-+.

592 Tsiklauri, D., Aug. 2007. A minimal model of parallel electric field generation in a trans-
593 versely inhomogeneous plasma. New Journal of Physics 9, 262-+.

594 Tsiklauri, D., Sakai, J.-I., Saito, S., Jun. 2005. Particle-In-Cell simulations of circularly
595 polarised Alfven wave phase mixing: A new mechanism for electron acceleration in
596 collisionless plasmas. Astronomy and Astrophysics 435, 1105-1113.

597 Volwerk, M., Louarn, P., Chust, T., Roux, A., de Feraudy, H., Holback, B., Jun. 1996.
598 Solitary kinetic Alfven waves: A study of the Poynting flux. Journal of Geophysical
599 Research (Space Physics) 101 (10), 13335-13344.

600 Watt, C. E. J., Rankin, R., Sep. 2008. Electron acceleration and parallel electric fields due
601 to kinetic Alfven waves in plasma with similar thermal and Alfven speeds. Advances in
602 Space Research 42, 964-969.

603 Watt, C. E. J., Rankin, R., Jul. 2010. Do magnetospheric shear Alfven waves generate
604 sufficient electron energy flux to power the aurora? Journal of Geophysical Research
605 (Space Physics) 115 (14), 7224-+.

run	m_i/m_e	cavity size	N_{mode}	$\delta B_{max}/B_0$
A	400	*no cavity*	8	0.0320
B	400	409.60× 1.20	8	0.0320
C	100	409.60× 1.20	8	0.0320
D	400	409.60× 1.20	1 (large)	0.0904
E	400	409.60× 1.20	1 (small)	0.0904
F	200	409.60× 1.20	8	0.0320

Table 1. Simulation parameters. $\delta B_{max}/B_0$ is set in order to have the same initial magnetic energy in all simulations.

Figure 1. Run A: temporal stack plot of the transverse electric field $E_y(x,t)$ along a field line (x horizontal axis).

Figure 2. Run B: map of the density at times (a) t =0, (b) t =179, and (c) t =409. The line corresponds to a curve of equation $y = Y(x,t)$ along the density gradient.

Figure 3. Run B: transverse electric field $E_y(x,t)$ along the curve $y = Y(x,t)$ shown on Fig 2. The time is on the vertical axis, and x is on the horizontal axis.

Figure 4. Run B: Map of the **perpendicular** electric field $E_y(x, y)$ at the same times as in Fig. 2.

Figure 5. Run B: Map of the parallel electric field $E_x(x, y)$ at the same times as in Fig. 2.

Figure 6. Run B: parallel electric field $E_x(x, t)$ along the curve $y = Y(x, t)$ shown on Fig 2. (Same axis as Fig. 3.)

Figure 7. Run B: electron distribution function $f_e(x, v_x)$ in logarithmic scale, along the curve $y = Y(x, t)$ shown on Fig 2. The horizontal axis is the position x and the vertical axis is the parallel velocity v_x.

Figure 8. Run B: energy fluxes of electrons (see Eq. 3) for $x = 102.4$. The flux F_{eu} (F_{ed}) is computed with the upgoing (downgoing) particles only, and F_{ecu} (F_{ecd}) with the upgoing (downgoing) particles in the middle half of the simulation box only.

Figure 9. Run B: energy fluxes of ions. Same computations as in Fig. 8, but for the ions.

Figure 10. Run E: electron distribution function $f_e(x, v_x)$, as in Fig. 7.

Figure 11. Maximal value of the parallel electric field, over the simulation box, as a function of time. The three curves correspond to simulations with different mass ratios. run B: $m_i/m_e = 400$, run F: $m_i/m_e = 200$, run C: $m_i/m_e = 100$.

Figure 12. Electron energy flux of downgoing electrons F_{ecd}, in the middle of the simulation box (see Fig. 8; **the red curves in both Figures are identical**). The three curves correspond to simulations with different mass ratios. run B: $m_i/m_e = 400$, run F: $m_i/m_e = 200$, run C: $m_i/m_e = 100$.

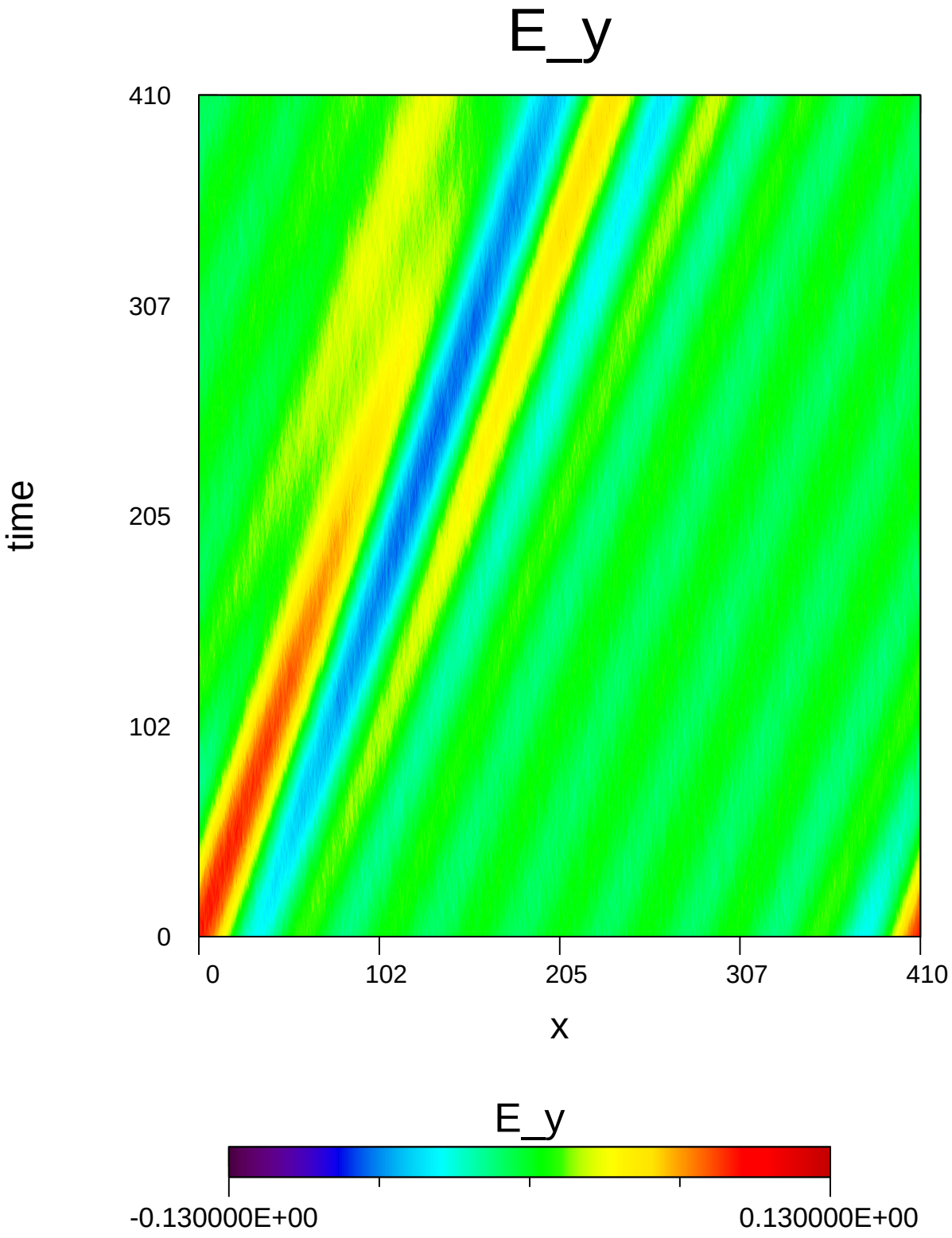
E_y
410
307
205
102
0
time
0
102
205
307
410
x
E_y
-0.130000E+00
0.130000E+00

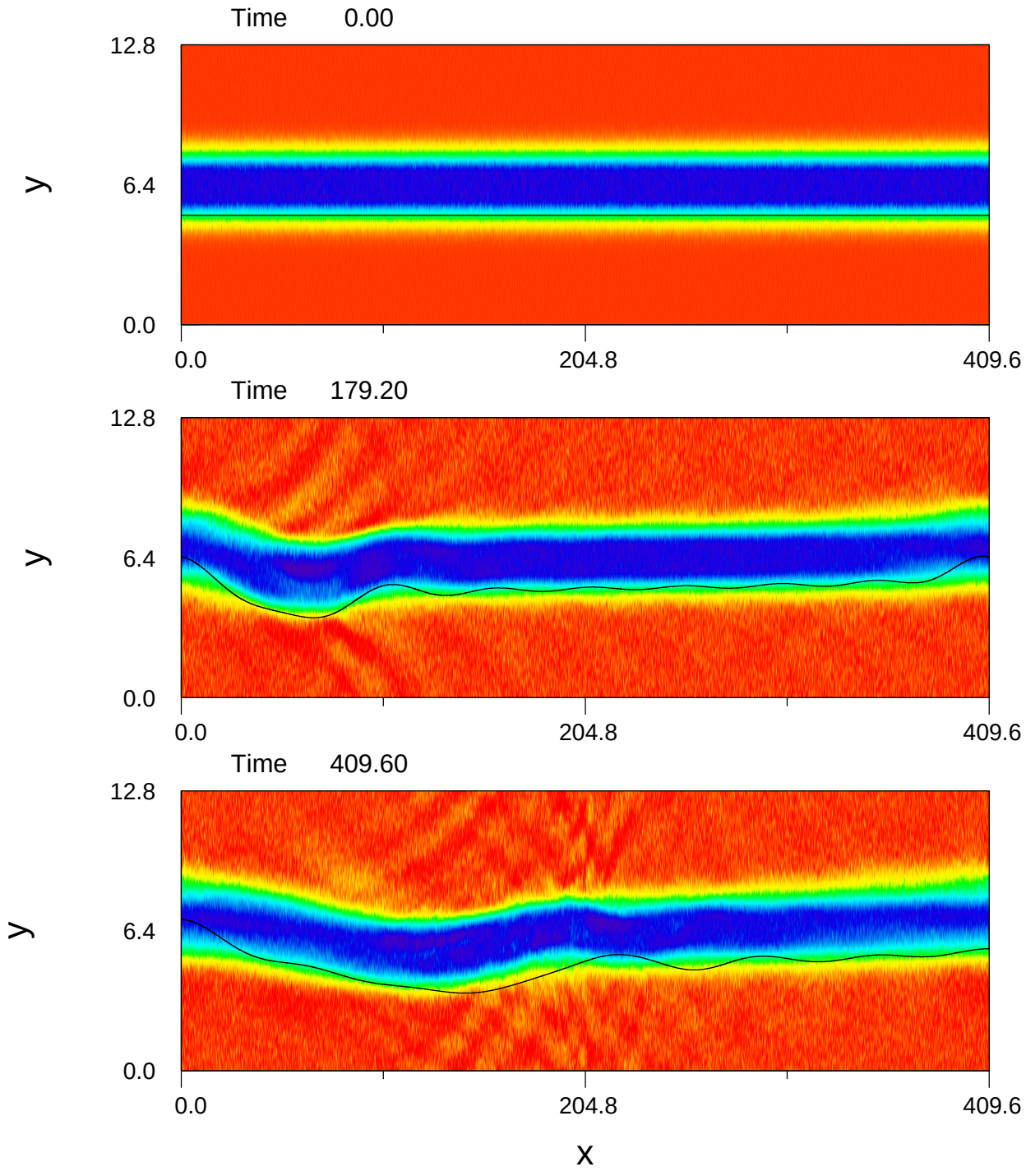
Time 0.00
Time 179.20
Time 409.60
12.8
6.4
0.0
y
0.0
204.8
409.6
x
n_e
0.000
1.500

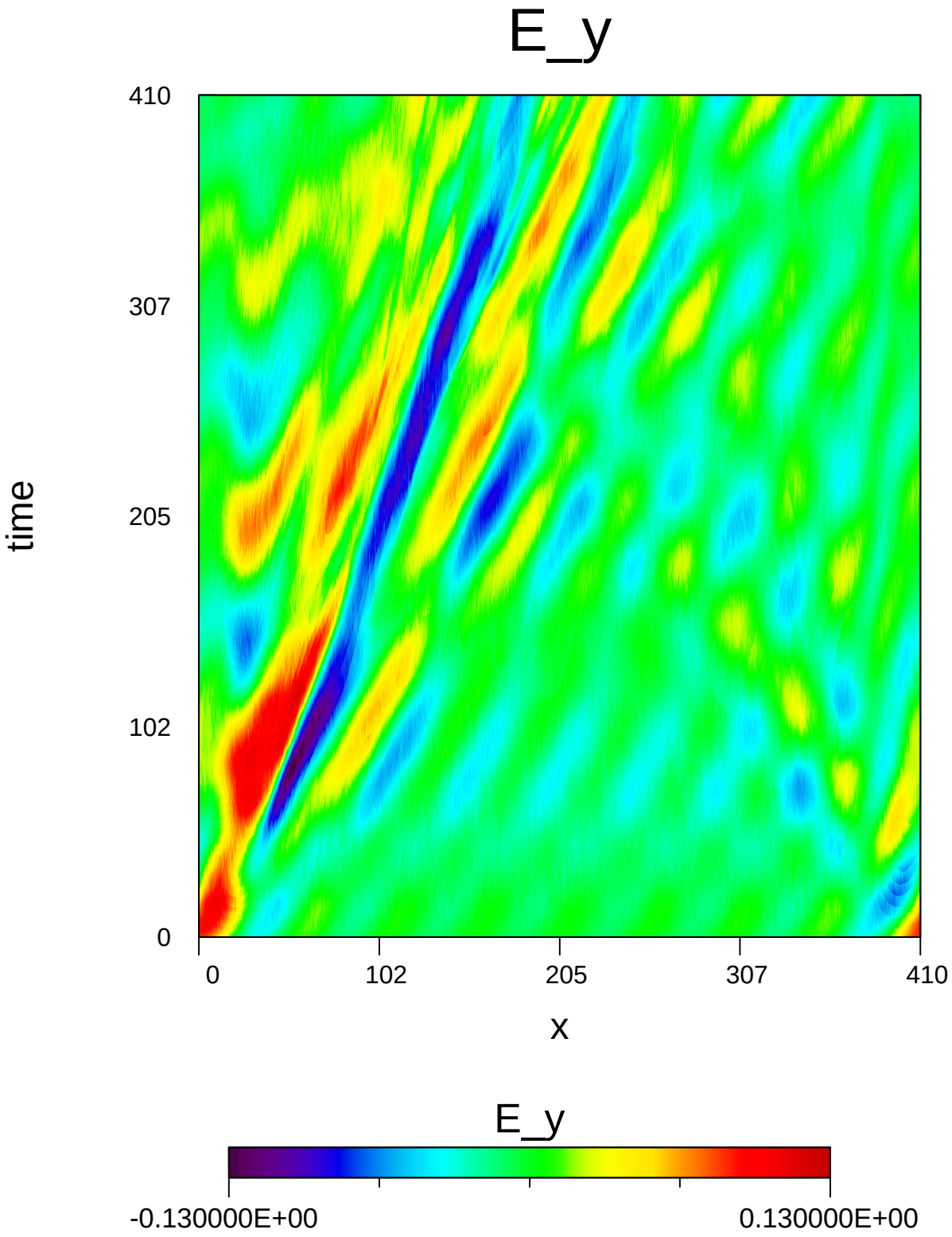
E_y
410
307
205
102
0
time
0
102
205
307
410
x
E_y
-0.130000E+00
0.130000E+00

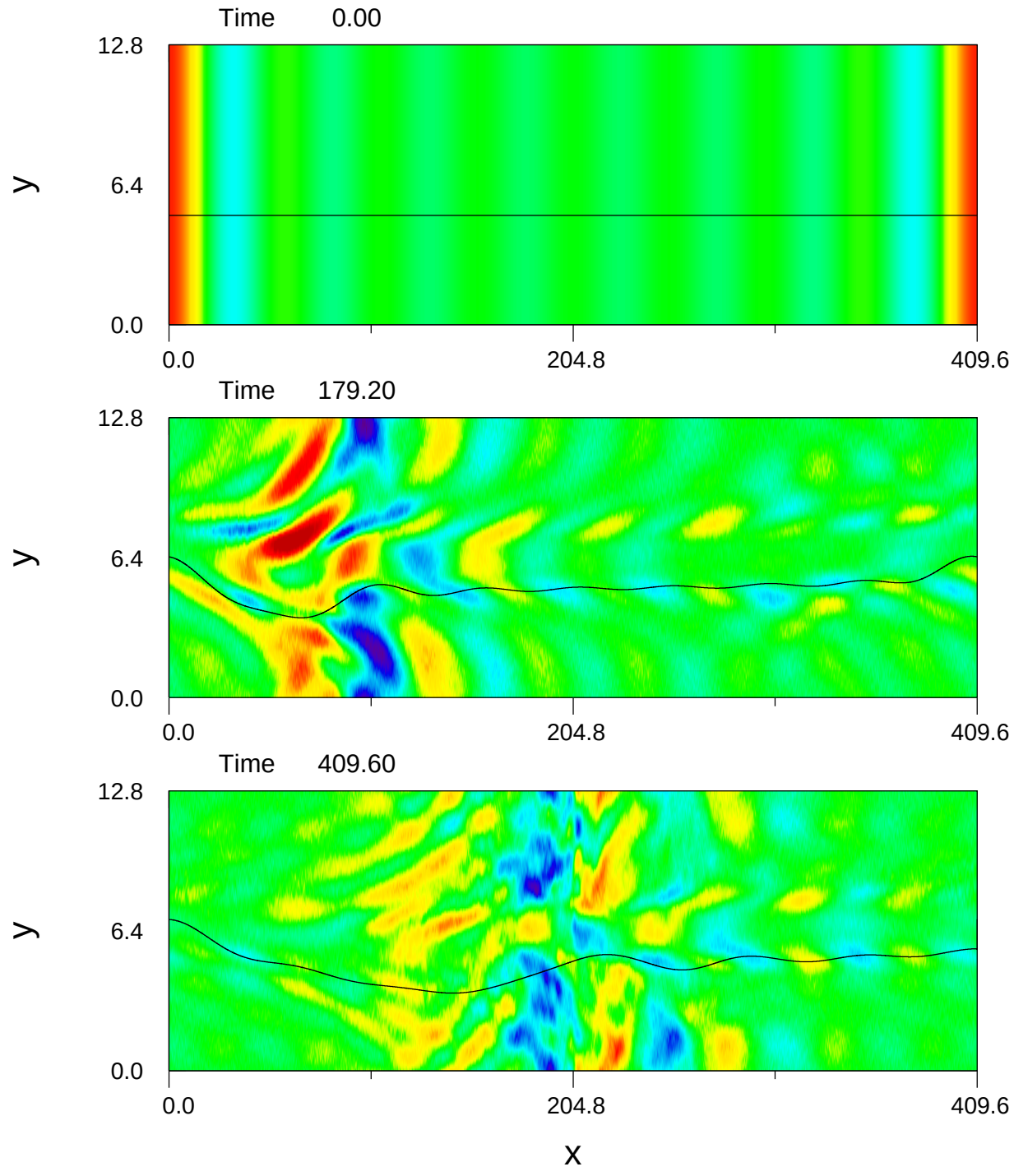
Time 0.00
12.8
6.4
0.0
y
0.0
204.8
409.6
Time 179.20
12.8
6.4
0.0
y
0.0
204.8
409.6
Time 409.60
12.8
6.4
0.0
y
0.0
204.8
409.6
x
E_y
-0.130000E+00
0.130000E+00

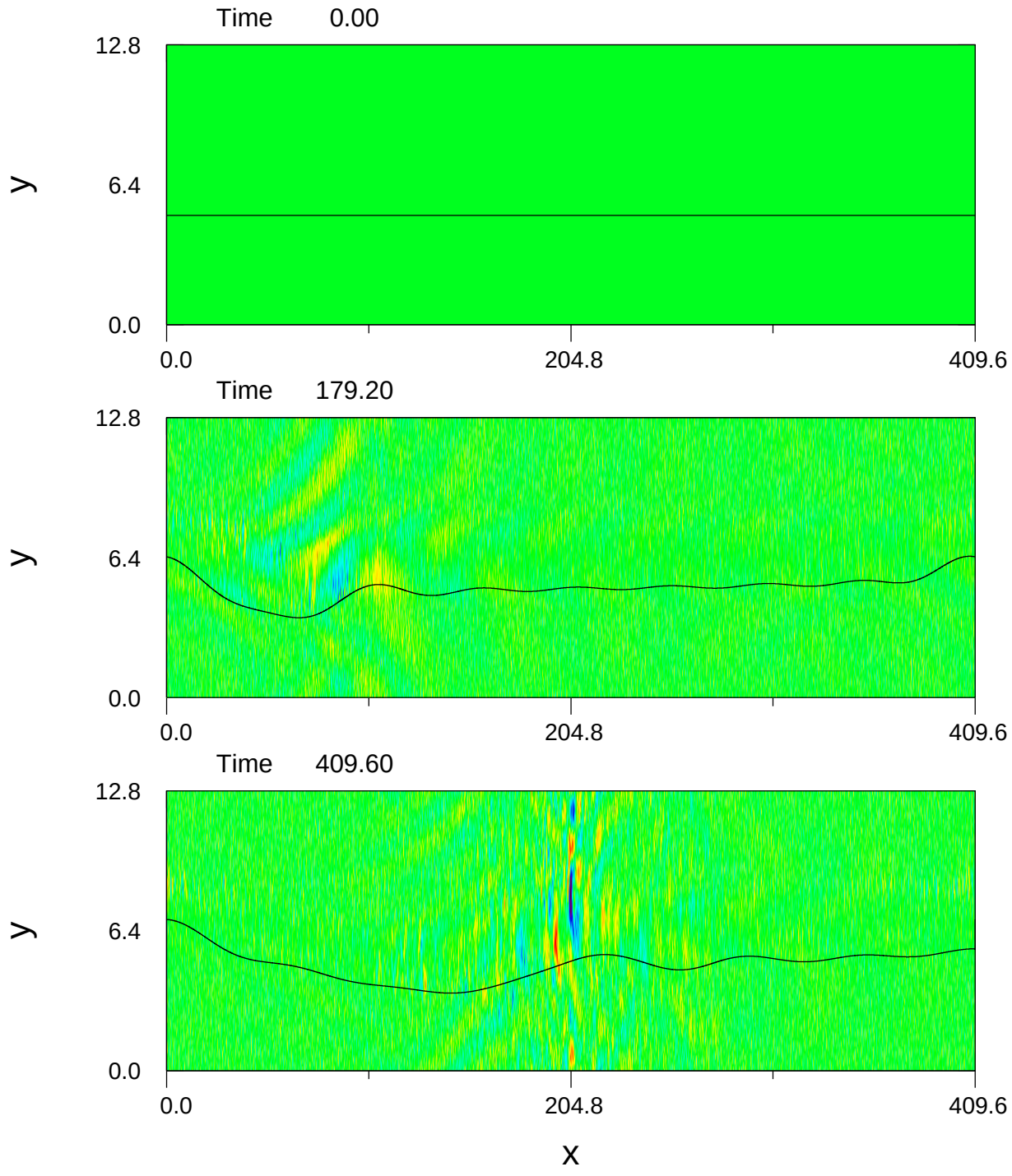
Time 0.00
12.8
6.4
0.0
y
0.0
204.8
409.6
Time 179.20
12.8
6.4
0.0
y
0.0
204.8
409.6
Time 409.60
12.8
6.4
0.0
y
0.0
204.8
409.6
x
E_x
-0.250000E-01
0.250000E-01

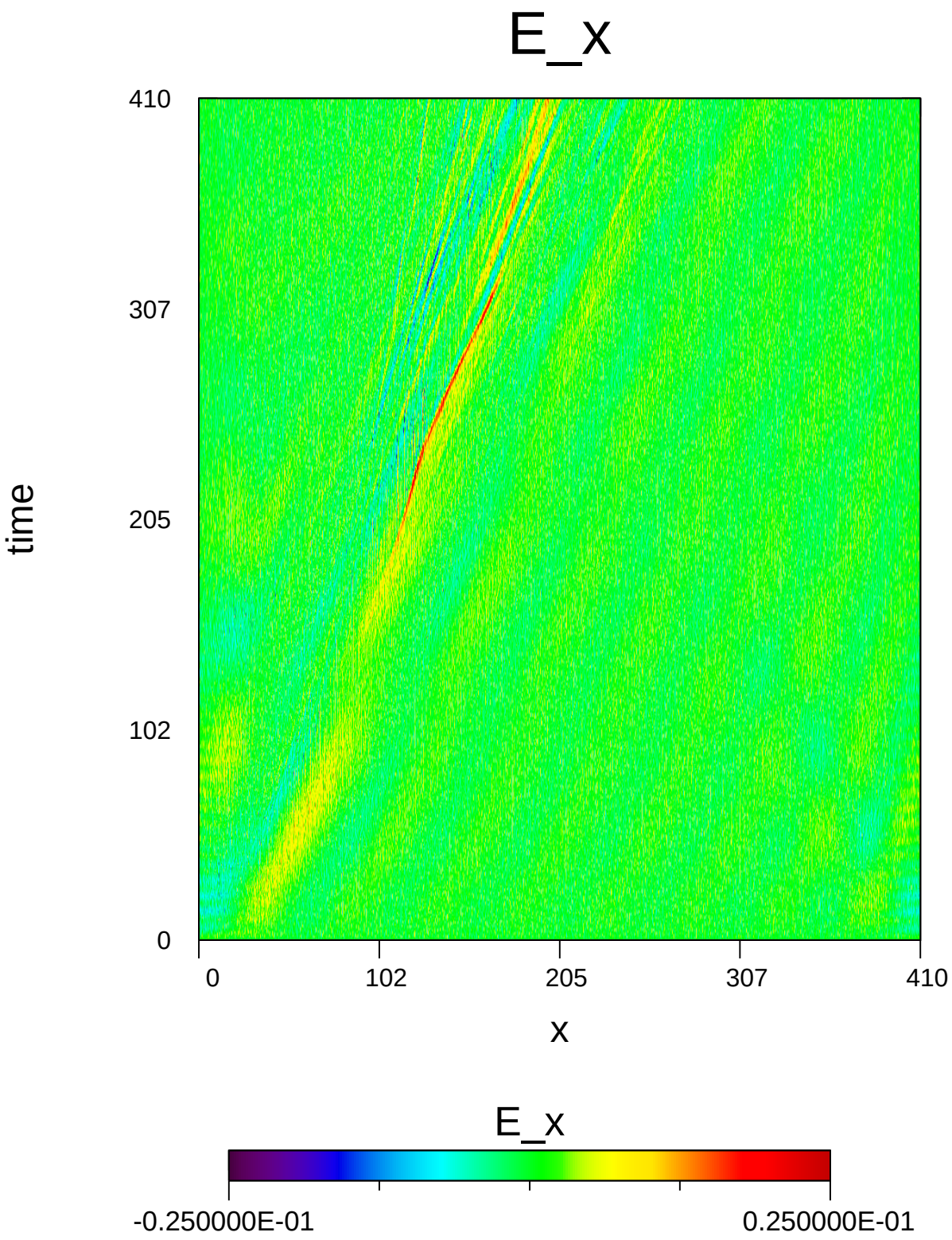
E_x
410
307
205
102
0
time
0
102
205
307
410
x
E_x
-0.250000E-01
0.250000E-01

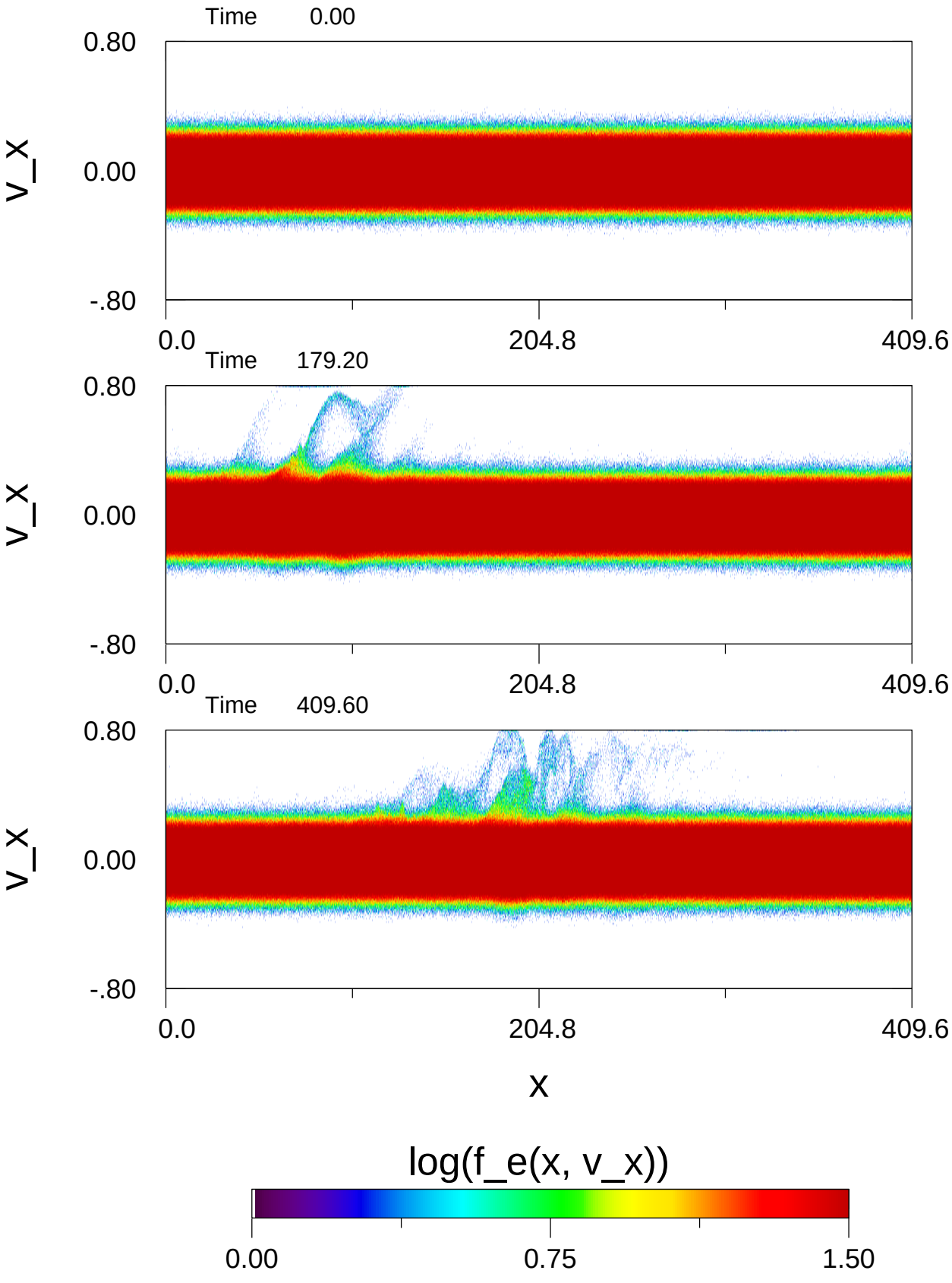
Time 0.00
0.80
0.00
-.80
v_x
0.0
204.8
409.6
Time 179.20
0.80
0.00
-.80
v_x
0.0
204.8
409.6
Time 409.60
0.80
0.00
-.80
v_x
0.0
204.8
409.6
x
log(f_e(x, v_x))
0.00
0.75
1.50

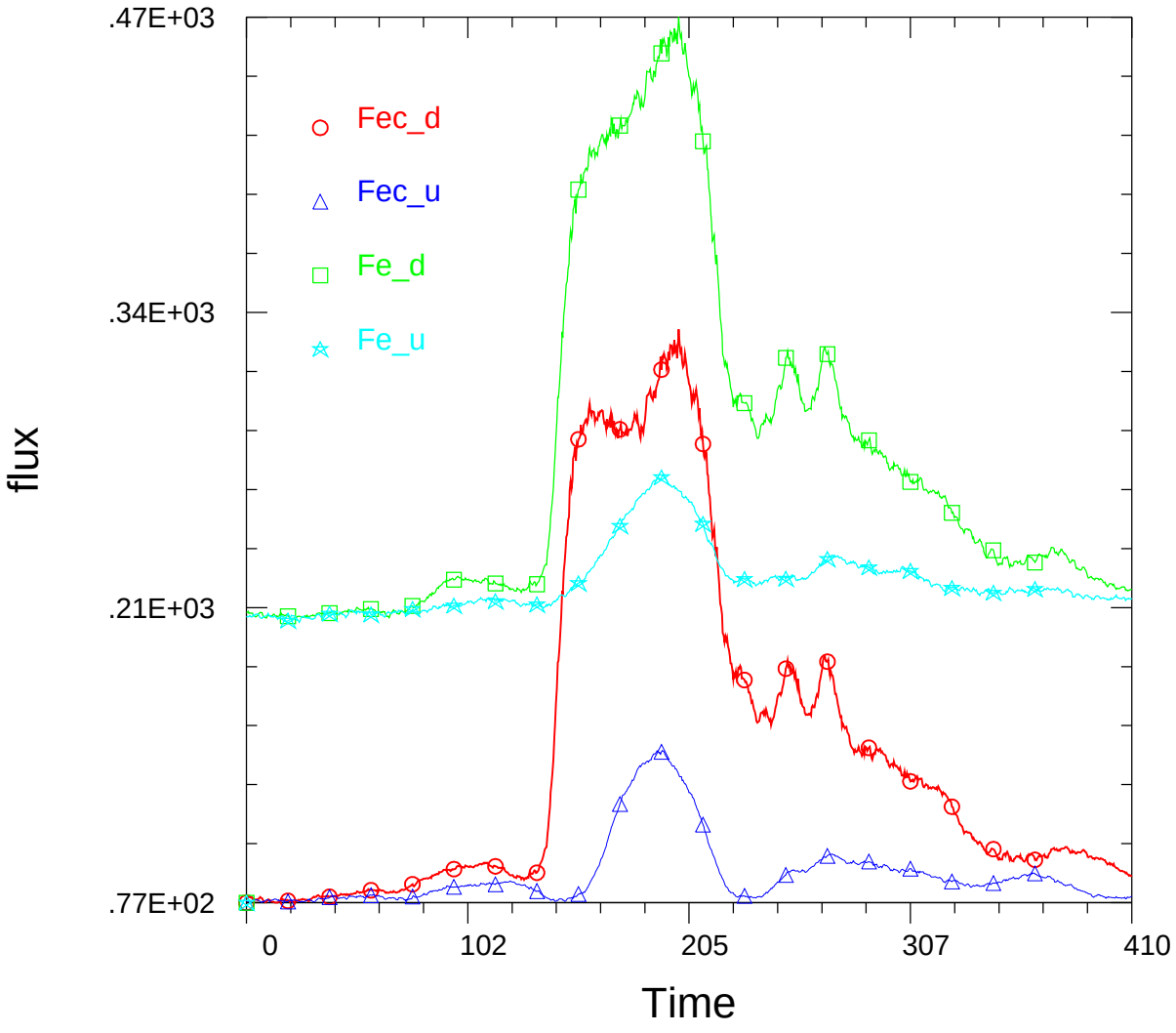
.47E+03
.34E+03
.21E+03
.77E+02
flux
Fec_d
Fec_u
Fe_d
Fe_u
0
102
205
307
410
Time

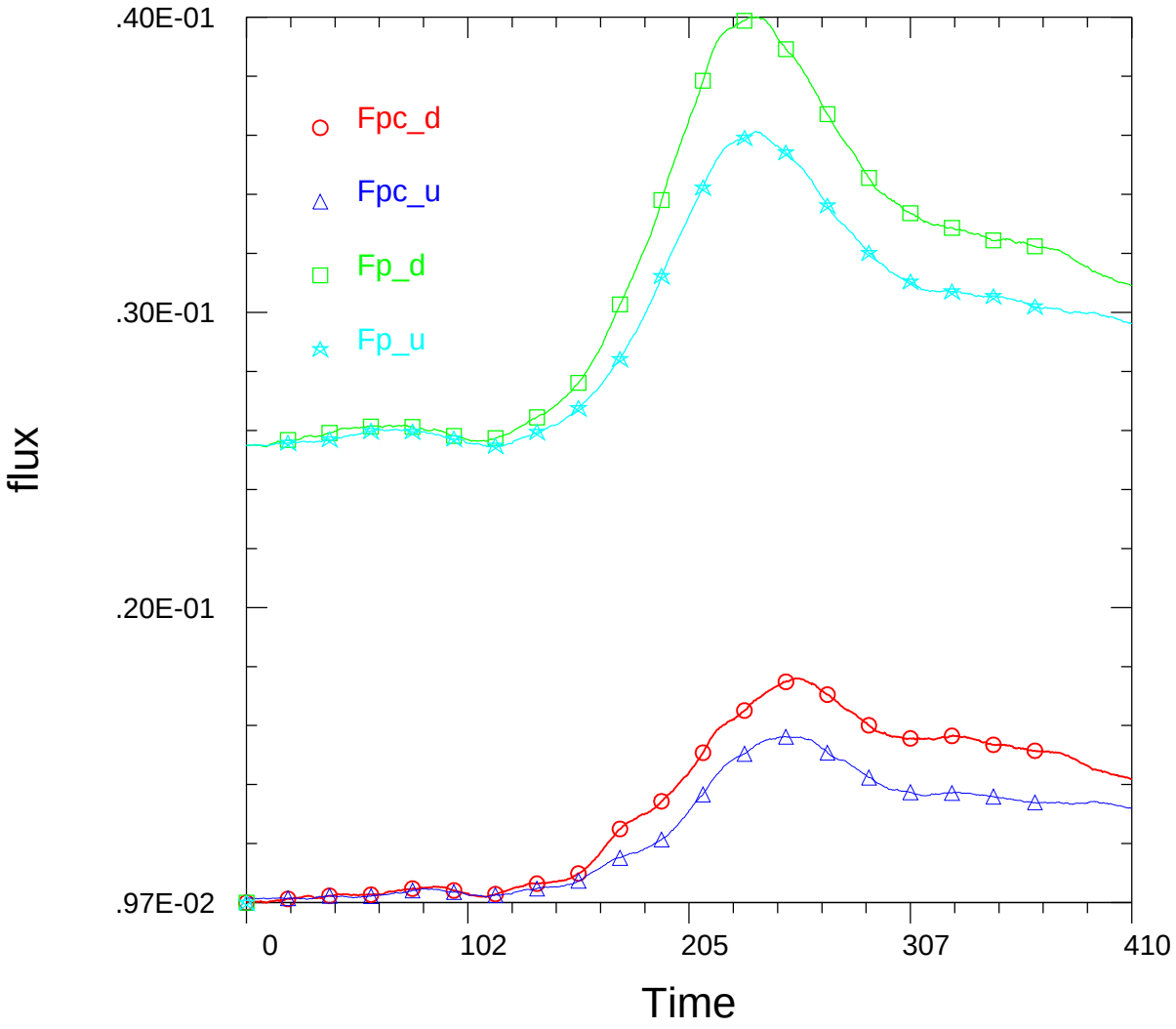
.40E-01
.30E-01
.20E-01
.97E-02
flux
Fpc_d
Fpc_u
Fp_d
Fp_u
0
102
205
307
410
Time

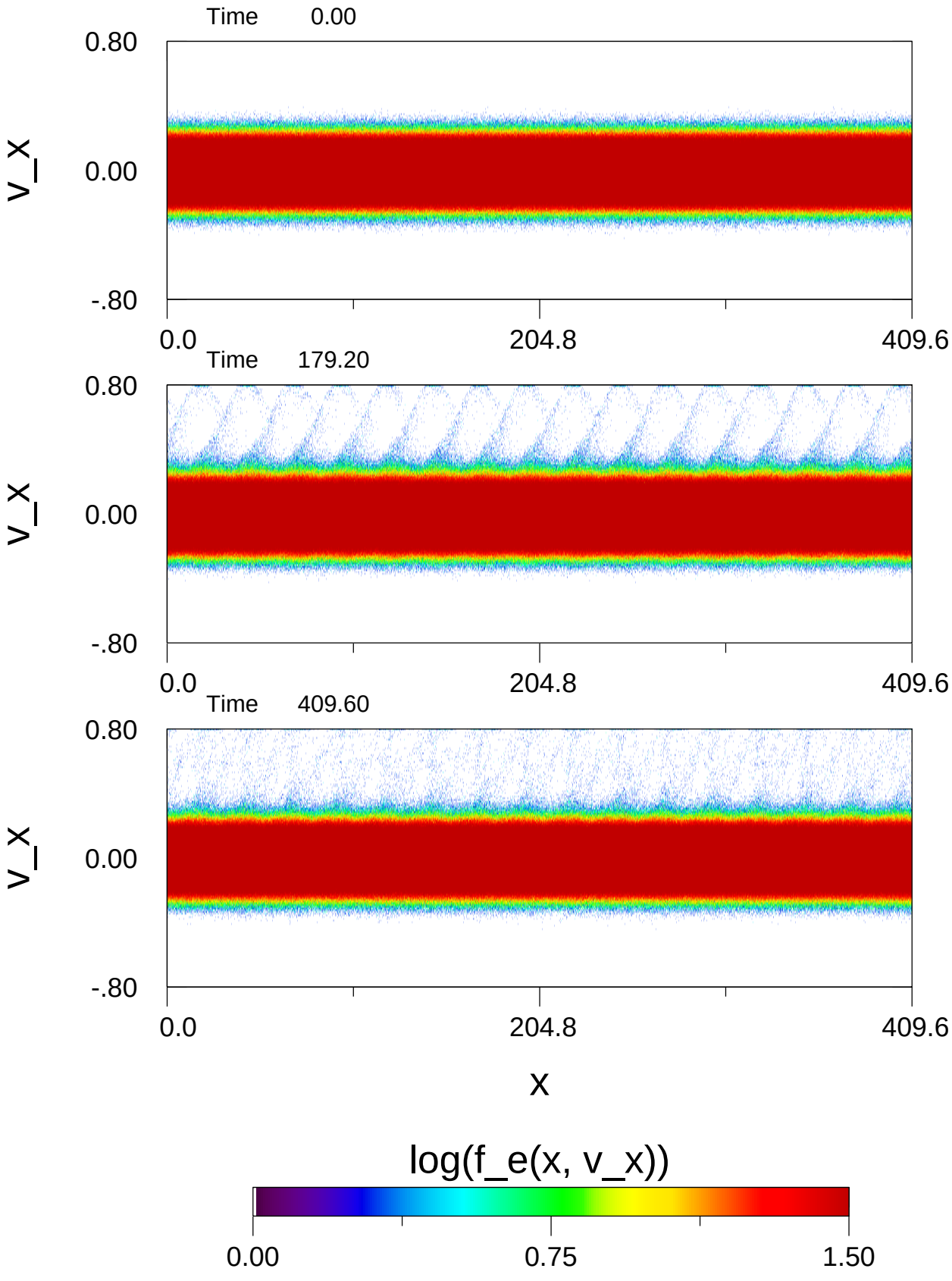
Time 0.00
0.80
0.00
-.80
v_x
0.0
204.8
409.6
Time 179.20
0.80
0.00
-.80
v_x
0.0
204.8
409.6
Time 409.60
0.80
0.00
-.80
v_x
0.0
204.8
409.6
x
log(f_e(x, v_x))
0.00
0.75
1.50

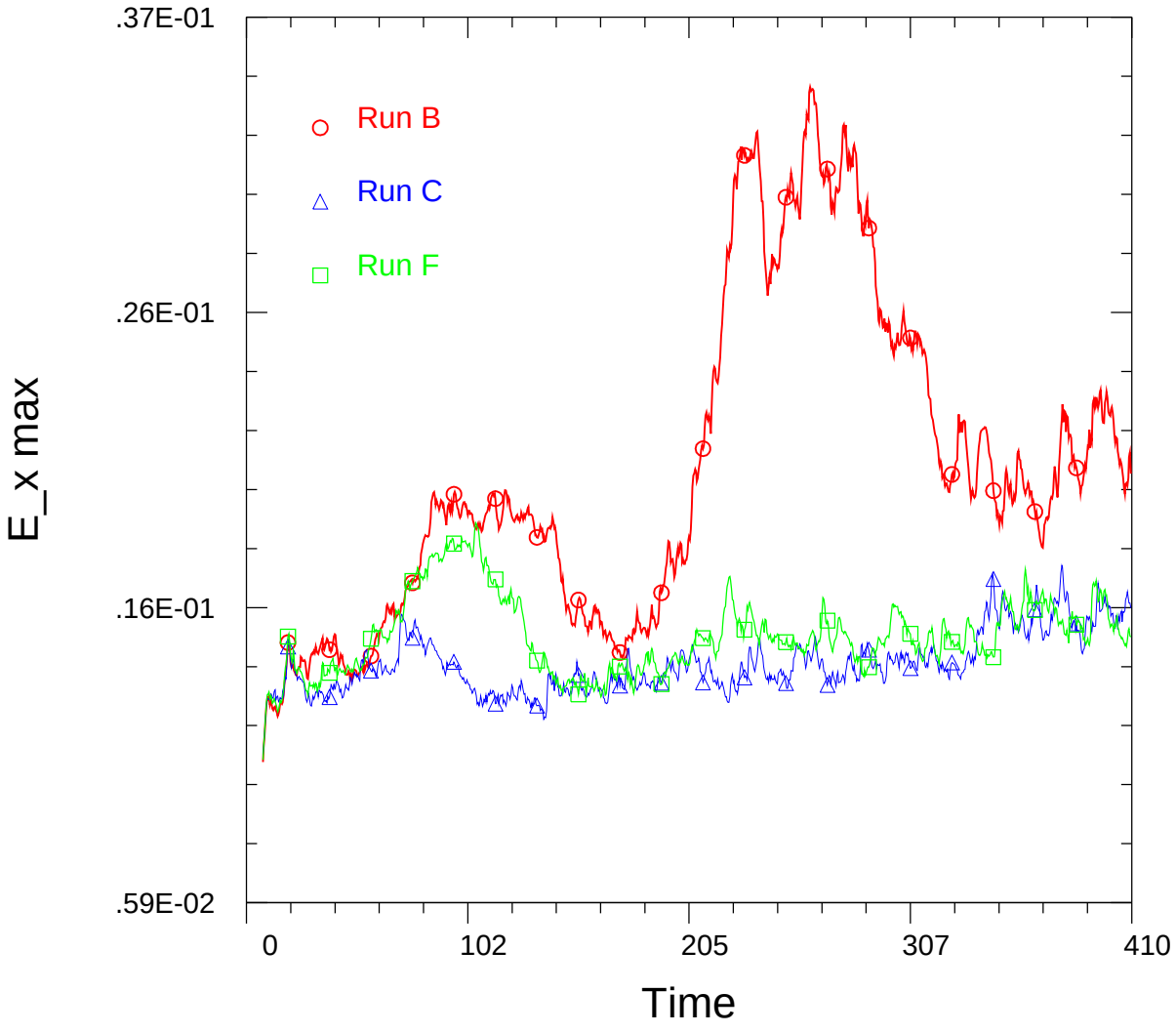
.37E-01
.26E-01
.16E-01
.59E-02
E_x max
Run B
Run C
Run F
0
102
205
307
410
Time

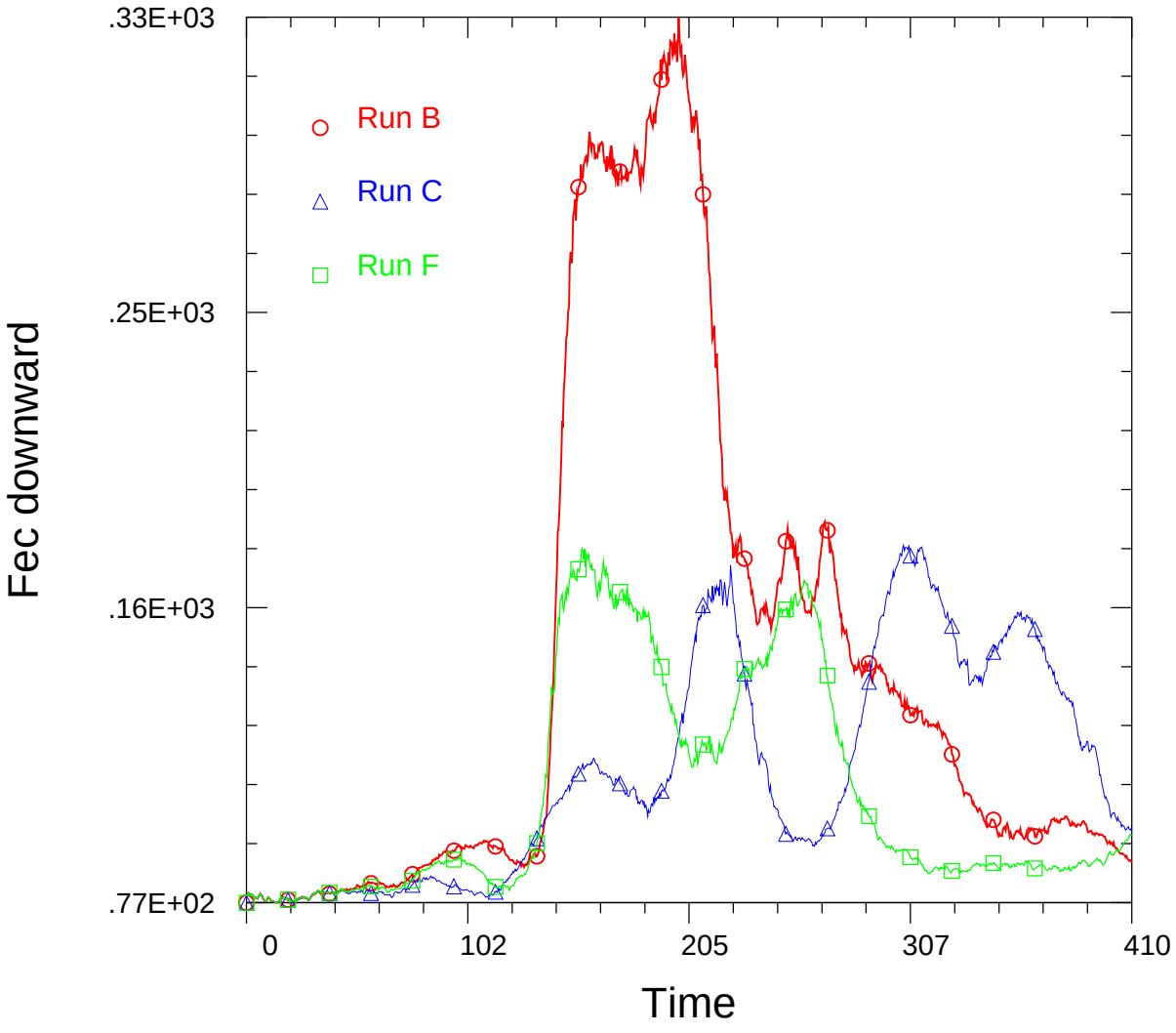
.33E+03
.25E+03
.16E+03
.77E+02
Fec downward
Run B
Run C
Run F
0
102
205
307
410
Time